Swiss Journal of Palaeontology

RESEARCH

Open Access

Natural assemblages of the earliest Triassic conodont *Hindeodus parvus* from the Shangsi section, Sichuan province, Southwest China

Jinyuan Huang[1,2,3*], Shixue Hu[1], Jun Li[1], Changyong Zhou[1], Qiyue Zhang[1], Wen Wen[1], Xiao Min[1], Haishui Jiang[4], Carlos Martínez-Pérez[2,5*] and Kexin Zhang[4]

Abstract

The morphology and number of elements in the Early Triassic conodont apparatus of the genus *Hindeodus,* particularly *Hindeodus parvus* (Kozur and Pjatakova, 1976), still remain controversial. In order to shed light on the apparatus composition of this iconic genus, here we report two well-preserved conodont natural assemblages of *Hindeodus* from the base of Member I of the Feixianguan Formation (Induan, lower Griesbachian, in age) at Shangsi section, Sichuan Province, Southwest China. These two natural assemblages preserve direct evidence of the number, morphology, and arrangement of elements in the apparatus of *Hindeodus,* and in particular *H. parvus*. The apparatus of *H. parvus* consists of six morphotype elements with S, M, and P positions, showing the typical ozarkodinid 15-element arrangement. The S_1-S_4 array comprises a set of nine ramiform elements: a crown-shaped alate element without a 'posterior' process situated at the S_0 position, two inner pairs of digyrate elements positioned at the S_{1-2} positions, and two outer pairs of bipennate elements located at the S_3 and S_4 locations. A pair of dolabrate elements occupy the M position outside the S array. The paired P_1 and P_2 positions are occupied by carminiscaphate and angulate elements, respectively. The 15-element apparatus architecture for the genus, resembles the well-known template of ozarkodinid model, further indicating the conservative architecture of the apparatus in Order Ozarkodinida spanning more than 250 million years.

Keywords Conodont, Natural assemblage, Multielement apparatus, 15-element, Early Triassic, Southwest China

Handling editor: Farid Saleh

*Correspondence:
Jinyuan Huang
hjinyuan69@qq.com
Carlos Martínez-Pérez
Carlos.Martinez-Perez@uv.es
[1] Chengdu Center, China Geological Survey (Geosciences Innovation Center of Southwest China), Chengdu 610281, China
[2] Cavanilles Institute of Biodiversity & Evolutionary Biology, University of Valencia, 46980 Valencia, Spain
[3] State Key Laboratory of Palaeobiology and Stratigraphy, Nanjing Institute of Geology and Palaeontology, Chinese Academy of Sciences, Nanjing 210008, China
[4] School of Earth Sciences, China University of Geosciences, Wuhan 430074, China
[5] School of Earth Sciences, University of Bristol, Life Sciences Building, Tyndall Avenue, Bristol BS8 1TQ, UK

Introduction

Conodonts are a group of jawless vertebrates that were widely distributed in various marine deposits from the Middle Cambrian to the Late Triassic characterized by a series of individual apatite pieces (Sweet & Donoghue, 2001). These pieces, the so-called conodont elements, were components of the feeding and complex apparatus located in the head region of these animals, that normally are recovered as isolated elements from the sediments (Aldridge et al., 1993). Commonly used for biostratigraphic correlation (Ferretti et al., 2020; Zhang et al., 2007; Zhao et al., 2008; among others) and paleoenvironmental interpretation (Sun et al., 2012, etc.), these elements are particularly important as index fossils (Henderson, 2018), and play a crucial role in the definition of

Springer Open

© The Author(s) 2024. **Open Access** This article is licensed under a Creative Commons Attribution 4.0 International License, which permits use, sharing, adaptation, distribution and reproduction in any medium or format, as long as you give appropriate credit to the original author(s) and the source, provide a link to the Creative Commons licence, and indicate if changes were made. The images or other third party material in this article are included in the article's Creative Commons licence, unless indicated otherwise in a credit line to the material. If material is not included in the article's Creative Commons licence and your intended use is not permitted by statutory regulation or exceeds the permitted use, you will need to obtain permission directly from the copyright holder. To view a copy of this licence, visit http://creativecommons.org/licenses/by/4.0/.

Global Stratotype Section and Point (GSSP) boundaries (Orchard, 2010), such as the global Permian–Triassic boundary (PTB) (Yin et al., 2001).

Conodont natural assemblages are fossils comprising several types of discrete elements, while they are mainly sampled isolated, conodont elements are sometimes found associated and juxtaposed on one bedding plane, forming a natural assemblage (Clark et al., 1981). These assemblages are crucial as they provide direct evidence of the element morphologies and positions within a conodont feeding apparatus, which are essential for discussing homology, taxonomy, and evolutionary relationships in conodonts (Donoghue et al., 2008; Purnell & Donoghue, 1998; Purnell et al., 2000; Sweet, 1988). In recent years, an increasing number of conodont fused clusters and natural assemblages have been reported worldwide, particularly from the Triassic Period in Asia. Notable examples include the genera *Hindeodus* (Agematsu et al., 2015, 2017; Zhang et al., 2017), *Clarkina* (Takahashi et al., 2019), *Hadrodontina* (Sun et al., 2020), *Neospathodus* (*Novispathodus*) (Goudemand et al., 2011, 2012), and *Scythogondolella* (Sun et al., 2021) in the Early Triassic; *Nicoraella* (Huang et al., 2019a, 2019b, 2019c, 2023) in the Middle Triassic; and *Mockina* (Demo et al., 2017; Zeng et al., 2021) in the Late Triassic. Additionally, the morphology, position, arrangement, and patterns of damage and microwear of these elements are fundamental for understanding the feeding mechanisms, function, ecology, and evolutionary relationships of conodont animals (Donoghue & Purnell, 1999; Donoghue et al., 2008; Martínez-Pérez et al., 2014, 2016; Purnell, 1995; Purnell & Jones, 2012; Purnell & Von Bitter, 1992).

Here, we describe two natural assemblages of the conodont genus *Hindeodus*, and in particular of the iconic species *H. parvus*, which preserve direct evidence of the element morphology, number, and arrangement of its feeding apparatus. *H. parvus* is a well-known species used to define the base of the Triassic period and so the boundary between the Paleozoic and Mesozoic eras (Kozur, 1996; Yin et al., 1986). The genus *Hindeodus* has a long stratigraphic range, extending from the Lower Carboniferous (Mississippian) to the lowermost Triassic (Kozur, 1996; Sweet, 1977). Notably, it underwent rapid evolution into more than 10 species during the late Permian to earliest Triassic (e.g., Jiang, 2008). This genus has been extensively studied to understand the crucial biostratigraphic interval of the Permian–Triassic Boundary (PTB) (Jiang et al., 2011; Kozur, 1989, 1995, 1996; among others).

The multielement apparatus of the genus *Hindeodus* was initially established by Sweet (1977), comprising six type elements. These include carmini- or anguliscaphate forms designated as the Pa (P_1) elements (*Spathognathodus cristulus*), angulate forms as the Pb (P_2) elements (*Ozarkodina curvata*), digyrate forms as the M elements (*Neoprioniodus camurus*), alate forms as the Sa (S_0) elements (*Hindeodus cristulus*), digyrate forms as the Sb (S_1 or S_2) elements (*Falcodus*? *alatoides*), and bipennate forms as the Sc (S_3 or S_4) elements (*Hindeodus* sp.). Surprisingly, neither Sweet (1977) nor Clark et al. (1981) and Sweet (1988) clearly specified the exact number of elements that constitute the multielement apparatus of the genus *Hindeodus*. Actually, the components of the apparatus in this genus is not well known due to the lack of well-preserved fossils of the fused clusters and natural assemblages. Consequently, most studies have focused primarily on their P_1 (Pa) elements. Among these species, *H. parvus* has been the most discussed based on their clusters and natural assemblages (Agematsu et al., 2015, 2017, 2018; Purnell et al., 2018; Zhang et al., 2017). Some natural assemblages of *Hindeodus* (i.e. species of *H. typicalis* and *H. parvus*) were reported from the lowermost Triassic strata in the Mino Terrane, Japan, identifying up to 13 elements in those assemblages (Agematsu et al., 2015). These included 7 S elements, 2 M elements, and 4 P elements, however, authors still proposed of a 15-element apparatus although no pair of S_1 elements were identified. This proposal was later supported by the presentation of a 15-element new natural assemblage studied using synchrotron radiation micro-tomography (SR-μCT) of Agematsu et al. (2017). At the same time, six fused clusters of the conodont *H. parvus* were described from bed 32 of the Shangsi section, suggesting a 13-element apparatus for *H. parvus*, with only one pair of P_1 elements (Zhang et al., 2017), therefore leaving open a controversy about the composition of its apparatus. In this context, we aim to re-examine the morphology and apparatus composition of the species *H. parvus* based on the newly discovered natural assemblages from the Shangsi section.

Geological setting

The conodont natural assemblages reported here were collected from a mudstone layer in the lowest part of the Feixianguan Formation at the Shangsi section in the Guangyuan City, Sichuan Province, Southwest China (Fig. 1A). The Shangsi section is located in Changjianggou (referred to as Shangjianggou in current maps) near Shangsi Village, Jiange County (Fig. 1B–D). This section was proposed as a potential Global Stratotype Section and Point (GSSP) for the Permian–Triassic Boundary (PTB), leading to extensive research efforts on biostratigraphy, geochemical, fossils, paleomagnetism, facies and event of the Permian–Triassic mass extinction, etc. (e.g. Chen et al., 2024; Jiang et al., 2011; Lai et al., 1996; Li et al., 1989; Song et al., 2013; among others).

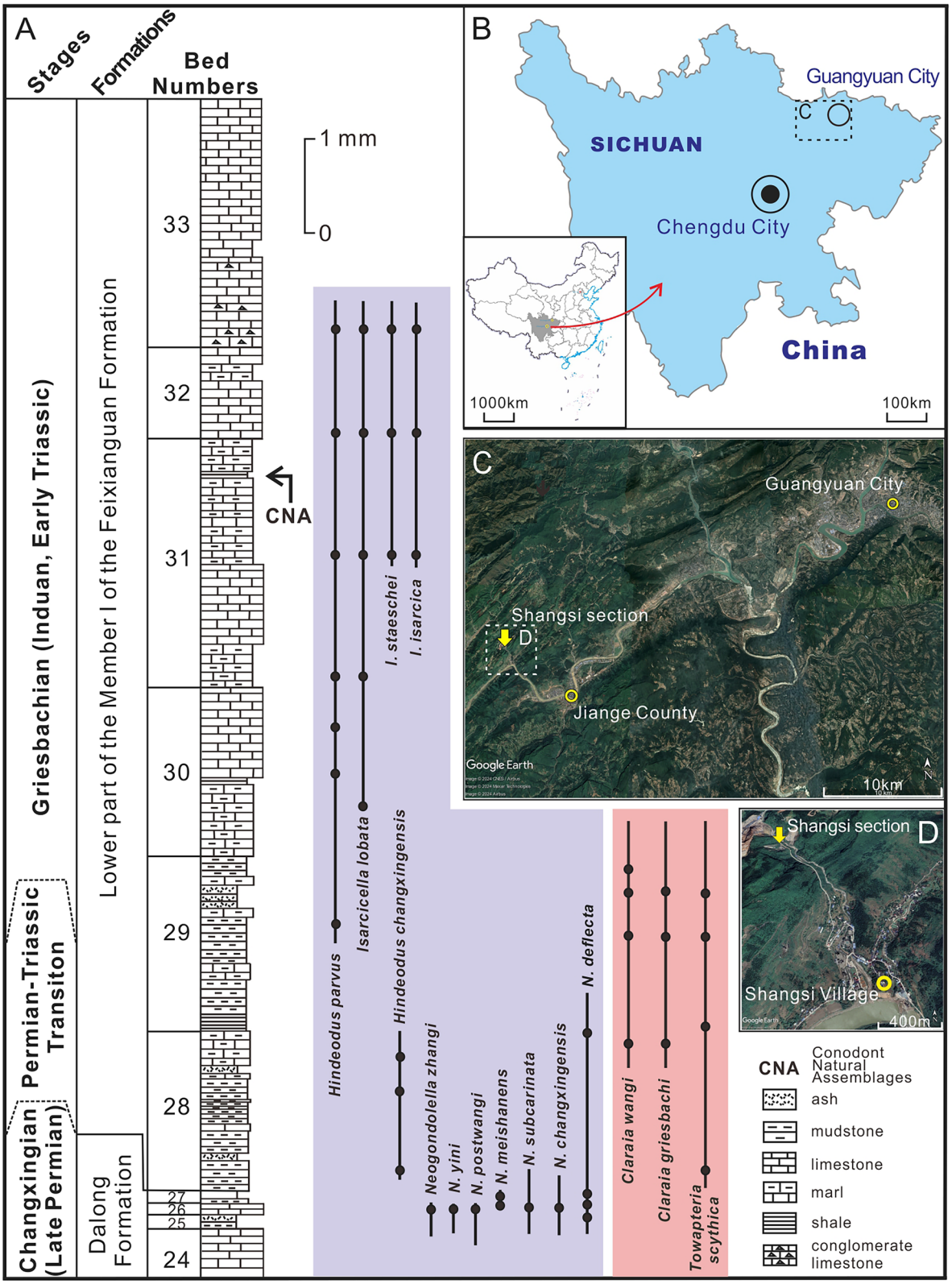

Fig. 1 Lithology and the location of the Shangsi section, Guangyuan City, Sichuan Province, southwest China (after Nicoll et al., 2002; Jiang et al., 2011 ; Hu et al., 2022), showing the fossil horizon of the conodont natural assemblages. **A**, lithological column of the Permian–Triassic transitional intervals and occurrence of index fossils of conodonts (pink blue area) and bivalves (pink area). **B–D**, index map of the Shangsi section

The Shangsi section is easily accessible and provides a continuous stratigraphic record from the Upper Permian Dalong Formation (Changhsingian) to Member I of the Lower Triassic Feixianguan Formation (Induan) (Fig. 1A) (Lai et al., 1996; Wignall et al., 1995, etc.). The Dalong Formation, characterized by siliceous limestone interbedded with shale, reflects a deep-water slope environment (Li et al., 1989). Fossils found in this formation, including brachiopods, bivalves, ammonoids, crinoids, radiolarians, and fish denticles, represent typical late Paleozoic marine communities (Li et al., 1989). Sedimentological studies indicate a progressive environmental shift from a deep basin to an upper slope during the Late Permian, transitioning to a tidal flat setting in the Early Triassic (Jiang et al., 2011; Lai et al., 1996).

The lower portion of the Lower Triassic Feixianguan Formation is primarily composed of thin-bedded marl, marlstone, mudstone, limestone, and shale (Fig. 1A). Fossil assemblages from the base of this formation include abundant bivalves, microconchids, conodonts, and a few ammonoids (Li et al., 1989). These assemblages are typical of early Triassic "disaster communities" that emerged following the Permian–Triassic mass extinction. This stratigraphic continuity and rich fossil content makes the Shangsi section an important site for studying the Permian–Triassic transition.

The conodont natural assemblages in this report come from the upper part of Bed 31 of the Shangsi section. According to previous conodont biostratigraphy studies, these assemblages could be assigned to the *Isarcicella isarcica* Zone, Induan (lower Griesbachian) in age (Jiang et al., 2011).

Materials and methods

Two well-preserved conodont natural assemblages (specimens Nos. 2023SSCNA1 and 2023SSCNA2) were obtained from a mudstone layer at the top of Bed 31 in Shangsi section, as shown in the Fig. 1. Both specimens are housed at the Chengdu Center, China Geological Survey (Geosciences Innovation Center of Southwest China). The part and counterpart of these two natural assemblages were photographed under different angled lighting using the Zeiss Smart Zoom 5 at the Chengdu Center, China Geological Survey. SEM images were taken with the Hitachi S-4800 at the same laboratory. Terminology for biological orientation and locational notation of the apparatus follows Purnell et al. (2000). The orientation of a single element and its processes uses traditional terms described by Clark et al. (1981), such as 'anterior', 'posterior', and 'lateral', indicated in quotation marks to distinguish them from biological orientations (rostral, caudal, dorsal, ventral, etc.) of Purnell et al. (2000).

The term 'fused clusters' refers to a group of elements that are fused or cemented together, often indicating conodont aggregation extracted from rocks. 'Natural assemblages' refer to the physical association of several types of discrete conodont elements on a bedding plane, interpreted as skeletal parts of one animal, with an emphasis on assemblages preserved on the surface of the layers (Clark et al., 1981).

Description of the natural assemblages

Specimen 2023SSCNA1 consists of eight elements within the part and counterpart (Figs. 2 and 3, respectively): five elements in the S array (one S_0 element and four sinistral S elements (S_1-S_4)), and three other elements (two P_2 elements and one M element). The feeding apparatus is collapsed from the sinistro-dextral orientation with a ventral component. The sinistral M element is positioned above the S elements, and the denticles of the P_2 elements are collapsed towards the rostral direction, indicating that the rostro-caudal axis is head down while the dorso-ventral axis is slightly inclined away from vertical relative to the sea surface. In this collapsed orientation, the dextral S elements will be covered by the sinistral elements. However, the paired P_1 elements of the apparatus are not observed in the specimen, possibly due to the burial in the matrix, or loss during diagenesis.

The symmetrical alate S_0 element (Fig. 2C, G), with a crown shape, lies on the rostral end of the S array. This element has a prominent cusp in the middle position and seven small denticles on both lateral processes. Four elements exhibit sinistral curvatures in the S_1 to S_4 positions of the apparatus, almost parallel alignment with their processes, and consistent orientation of their cusps and denticles. Based on the topological evidence and homology, the outermost bipennate element with the longer 'posterior' process is identified as the S_4

(See figure on next page.)

Fig. 2 Conodont natural assemblage of *H. parvus*. Collection number 2023SSCNA1 part, the sample comes from the Bed 31. **A–B**, photographs were taken using a stereomicroscope under different angles of incident lights. **C–D**, SEM photograph of the whole conodont natural assemblage, and its corresponding outline drawing, the solid lines represent the edges of the solid conodont elements, while the dashed lines represent the edges of the mouldic conodont elements. **E**, the enlarged S-M part of the natural assemblage, showing the ramiform elements. **F**, the P_2 element. **G**, the S_0 element. All scale bars represent 200 μm. Brick red represents P_1 elements; chartreuse: P_2; green: S_0; brown: S_1; red: S_2; purple: S_3; orange: S_4; blue: M elements; respectively

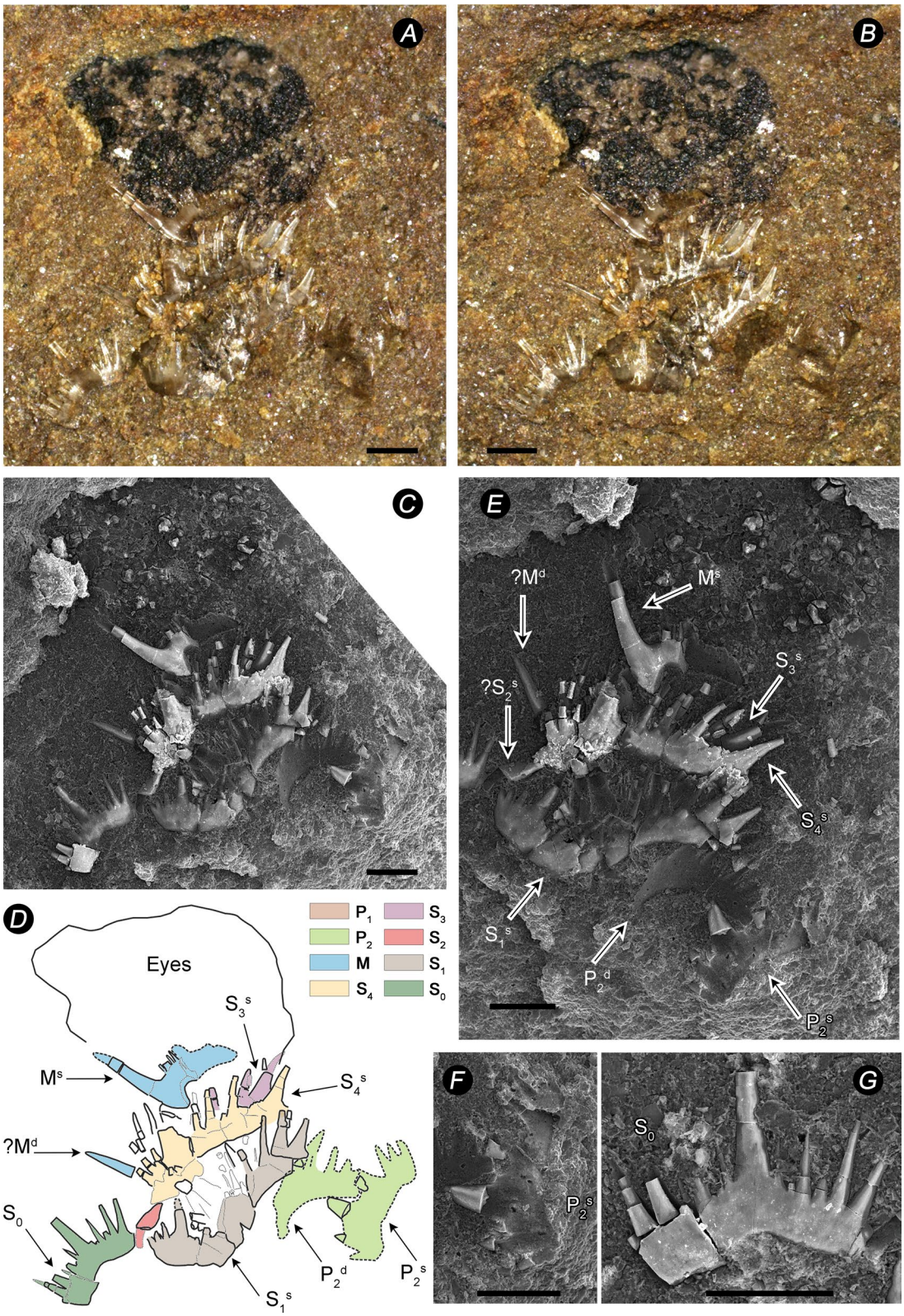

Fig. 2 (See legend on previous page.)

element (Fig. 2E). The S_3 element is mostly covered by the S_4 element (Fig. 2E), revealing only the denticles of its 'posterior' process. The S_2 element only retains its 'long lateral' process (Fig. 3C, D). The digyrate S_1 element is characterized by a long and substraight 'posterior' process (oriented towards the caudodorsal direction in the assemblage) (Fig. 2E), and a short, 'laterally' incurved 'anterior' process (oriented towards the dextral side in the assemblage) (Fig. 2E).

One dolabrate M element is broken into two pieces, with one piece preserved on the part (Fig. 2E) and the other on the counterpart (Fig. 3F). It settled above and parallel to the sinistral S elements, indicating that it is a sinistral M element. A possible cusp remain of the dextral M element located at the rostral of sinistral S_4 element (Fig. 2D). This element has a long, prominent cusp and a faint anticusp.

A pair of angulate elements in the P_2 position are located very close to the distal end of the S elements (Figs. 2E, 3C). Both the dextral and sinistral P_2 elements show a slight flexion pointing caudally (Fig. 3E).

Specimen 2023SSCNA2 comprises at least 12 elements in S, M, and P positions (Figs. 4, 5 respectively part and counterpart). Based on the curvatures of the elements and their topological positions within the apparatus, we can identify both, the dextral and sinistral elements in the assemblage. The feeding apparatus is collapsed from the sinistro-dextral orientation with some rostral and ventral components. The sinistral S elements and P elements are offset to some extent from the dextral elements, and the denticles of the P_2 elements are positioned against each other, indicating that the rostro-caudal axis is head up, while the dorsoventral axis is inclined away from vertical relative to the sea surface. However, some elements, such as the S_0 element and the sinistral M element of the apparatus, are not observed in the specimen, possibly due to the burial in the matrix, or loss during diagenesis.

A dolabrate M element is positioned on the dorsal part of the assemblage, featuring a long cusp (Figs. 4E, 5F). The posterior process is preserved in the part (Fig. 4E), and the anterior cusp is visible in the counterpart (Fig. 5F). The lower margin of the 'posterior' process is nearly parallel to the adjacent S_4 and S_3 elements. Based on its curvature, it is identified as a dextral M element.

The dextral bipennate S_4 element (Fig. 5F) is located on the inner side of the dextral M element. It is robust, with a long 'posterior' process and a short 'lateral' flexed 'anterior' process (Fig. 5F). Adjacent to this S_4 element there is a bipennate S_3 element of similar size and proportions, with a slightly shorter 'anterior' process curved 'laterally' (Fig. 4E). The dextral S_2 and S_1 elements could be partially identified by their juxtaposed short curvature of their 'lateral' processes, indicating that these two elements have a similar shape. Two sinistral S_4 and S_3 elements could be identified by their long 'posterior' processes and prominent main cusps (Fig. 4E). A possible long 'lateral' process remnant of the sinistral S_1 element is preserved distally to the dextral S elements (Fig. 5F). No S_0 element has been identified at the specimen.

A pair of angulate P_2 elements are located very close to and beneath the S array (Fig. 4E). These elements are slightly curved, with their concave sides pointing caudally. These two P_2 elements are different from the P_2 elements in 2023SSCNA1 (Fig. 2, 3) in terms of the number of denticles and the second-order denticles in the dextral element.

At the caudal end of the assemblage, two carminiscaphate P_1 elements are juxtaposed with a prominent cusp, slightly displaced from each other (Fig. 4D, 5D). Based on the morphology of their high and robust cusps, the 'lateral' expanding basal cavity at the 'posterior' half, smooth 'upper surface', and the high 'posterior' edge, these two P_1 elements can be identify as belonging to *H. parvus*. However, due to the absence of the P_1 element in specimen 2023SSCNA1 and the slight morphological differences in its P_2 element compared to specimen 2023SSCNA2, we cannot definitively determine that specimen 2023SSCNA1 belongs to *H. parvus*. Nevertheless, given the strong morphological similarities in the M elements and the $S_{1\text{-}2}$ and $S_{3\text{-}4}$ elements, we tentatively assign specimen 2023SSCNA1 to *H.* ex gr. *parvus*.

Hindeodus parvus apparatus composition

None of the two studied conodont natural assemblages in our collection contain the remains of all count the 15 elements of a complete *Hindeodus* apparatus. However, the P_1 and P_2 elements are paired, along with a complete symmetrical pair of S_3 and S_4 elements, and the S_0 element is symmetrical by itself. This indicates that our

(See figure on next page.)

Fig. 3 Conodont natural assemblage of *H. parvus*. Collection number 2023SSCNA1 counterpart, the sample comes from the Bed 31. **A–B**, photographs are took by stereomicroscope under the different angle incident lights. **C–D**, SEM photograph of the whole conodont natural assemblage, and its corresponding outline drawing, the solid lines represent the edges of the solid conodont elements, while the dashed lines represent the edges of the mouldic conodont elements. **E**, the pair of P_2 elements. **F**, the M element. All scale bars represent 200 μm. The color coding is as described in Fig. 2

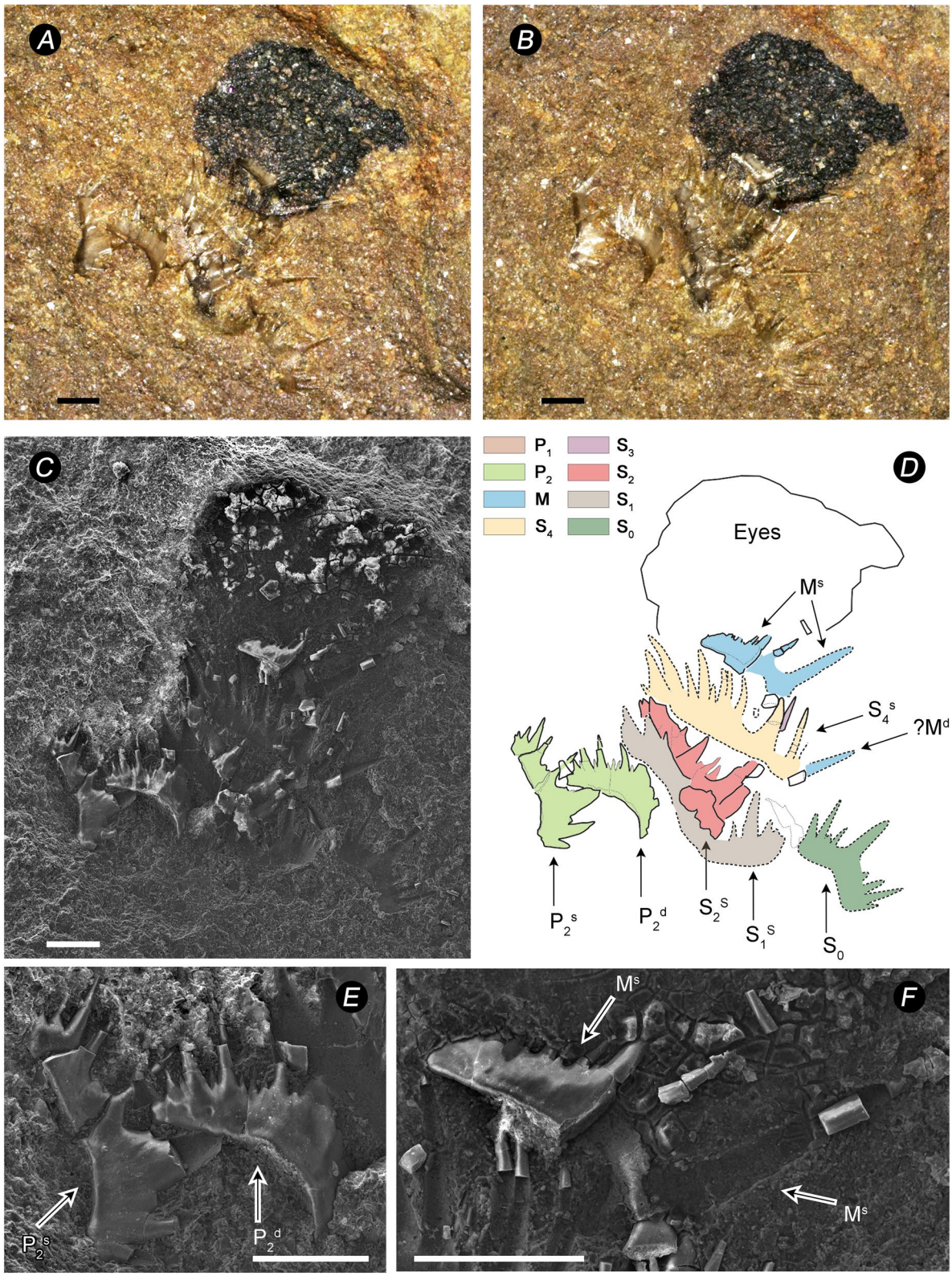

Fig. 3 (See legend on previous page.)

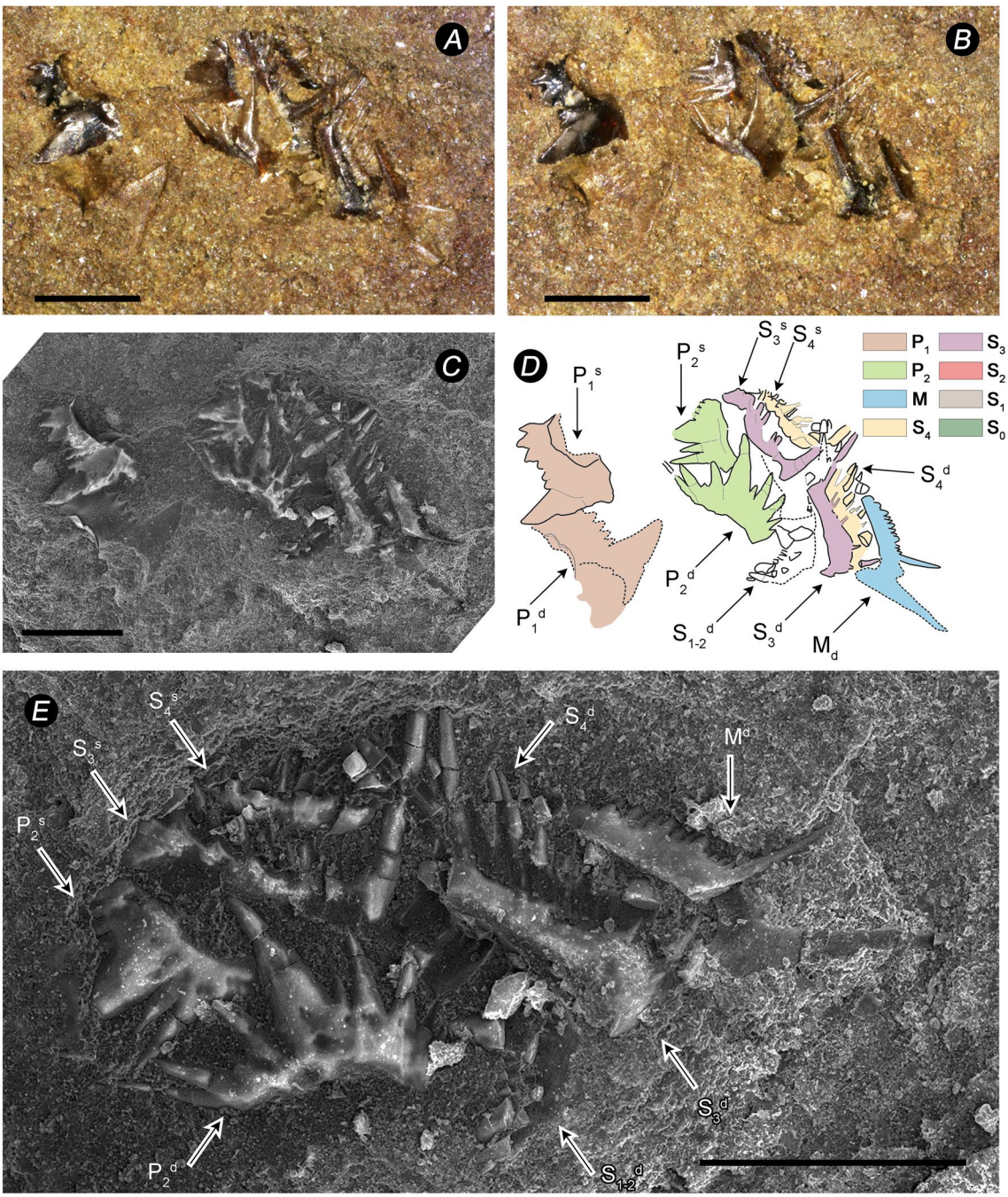

Fig. 4 Conodont natural assemblage of *H. parvus*. Collection number 2023SSCNA2 part, the sample comes from the Bed 31. **A–B**, photographs were taking by stereomicroscope under the different angle incident lights. **C–D**, SEM photograph of the whole conodont natural assemblage, and its corresponding outline drawing, the solid lines represent the edges of the solid conodont elements, while the dashed lines represent the edges of the mouldic conodont elements. **E**, the enlarged S-M elements and paired P_2 elements. All scale bars represent 500 μm. The color coding is as described in Fig. 2

feeding apparatus also has a symmetrical architecture, similar to other ozarkodinid apparatuses. Therefore, the S_1, S_2, and M elements should also be paired. Based on the characteristic of symmetrical architecture in the feeding apparatus, our data indicates that the apparatus of *H. parvus* is composed by 15 elements. It includes an alate S_0 element and pairs of S_1, S_2, S_3, S_4, M, P_2, and P_1 elements (Fig. 6).

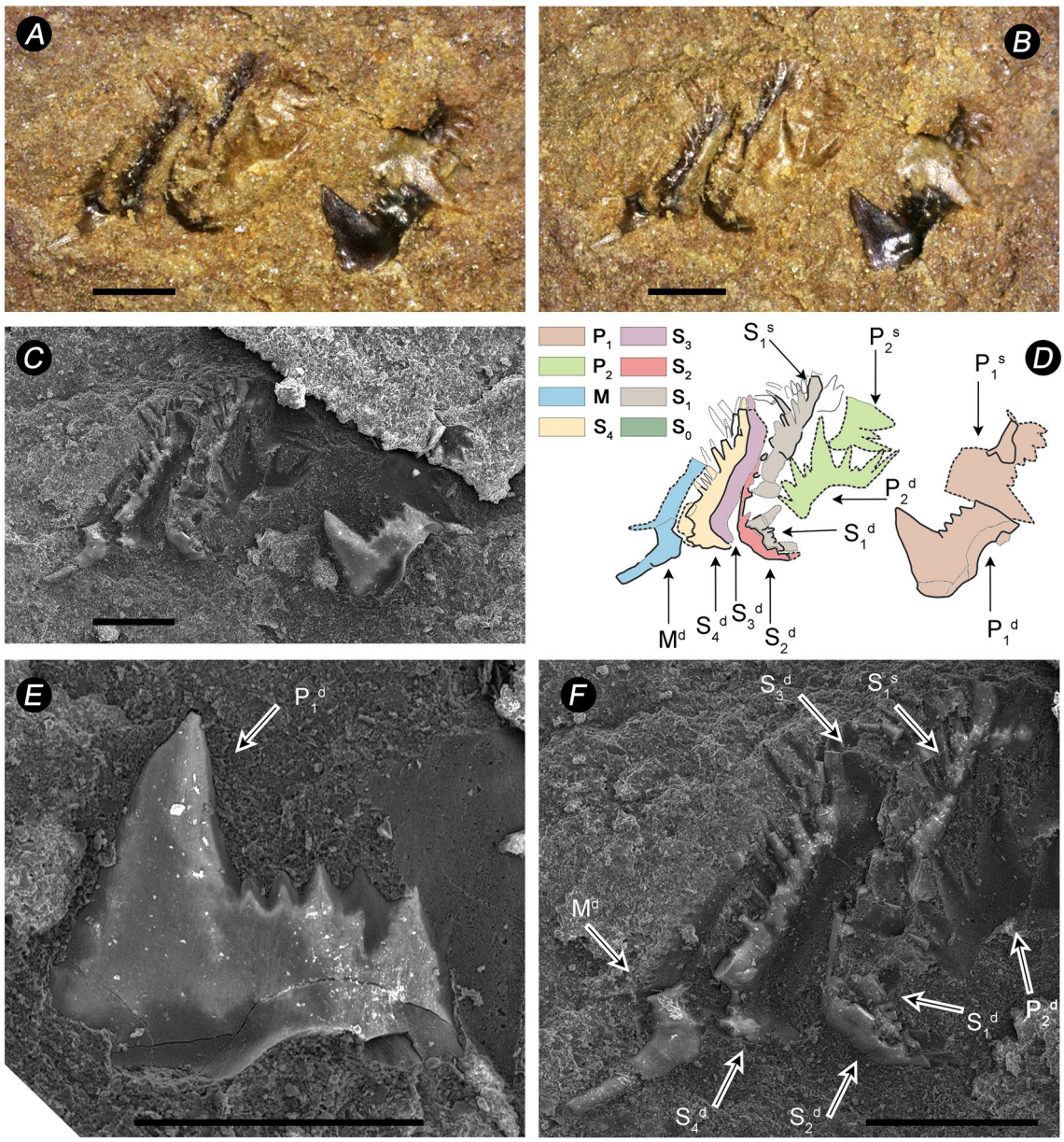

Fig. 5 Conodont natural assemblage of *H. parvus*. Collection number 2023SSCNA2 counterpart, the sample comes from the Bed 31. **A–B**, photographs were taking by stereomicroscope under the different angle incident lights. **C–D**, SEM photograph of the whole conodont natural assemblage, and its corresponding outline drawing, the solid black lines represent the edges of the conodont elements, while the dashed lines represent the edges of the mouldic conodont elements. **E**, the P_1 element. **F,** the enlarged S-M elements. All scale bars represent 400 μm. The color coding is as described in Fig. 2

The S_0 element is an alate form, bilaterally symmetrical, crown shape, bearing a long cusp, but lacking a 'posterior' process, six small denticles on each 'lateral' process (Fig. 2G). Although we cannot confirm the development of a 'posterior' process in the assemblage, this unique S_0 element shape is known from other natural assemblages and from discrete elements assigned to *Hindeodus* (Agematsu et al., 2015, 2017; Li et al., 1989; Zhang et al., 2017), providing strong evidence to our assignment.

The S_1 and S_2 elements both have a similar shape. The elements are laterally compressed and have a long cusp with two unequal long processes. The denticles are delicate except for the distalmost two denticles on the long 'posterior' process (oriented caudally) and one denticle is large on the relatively 'short lateral' process. It is hard

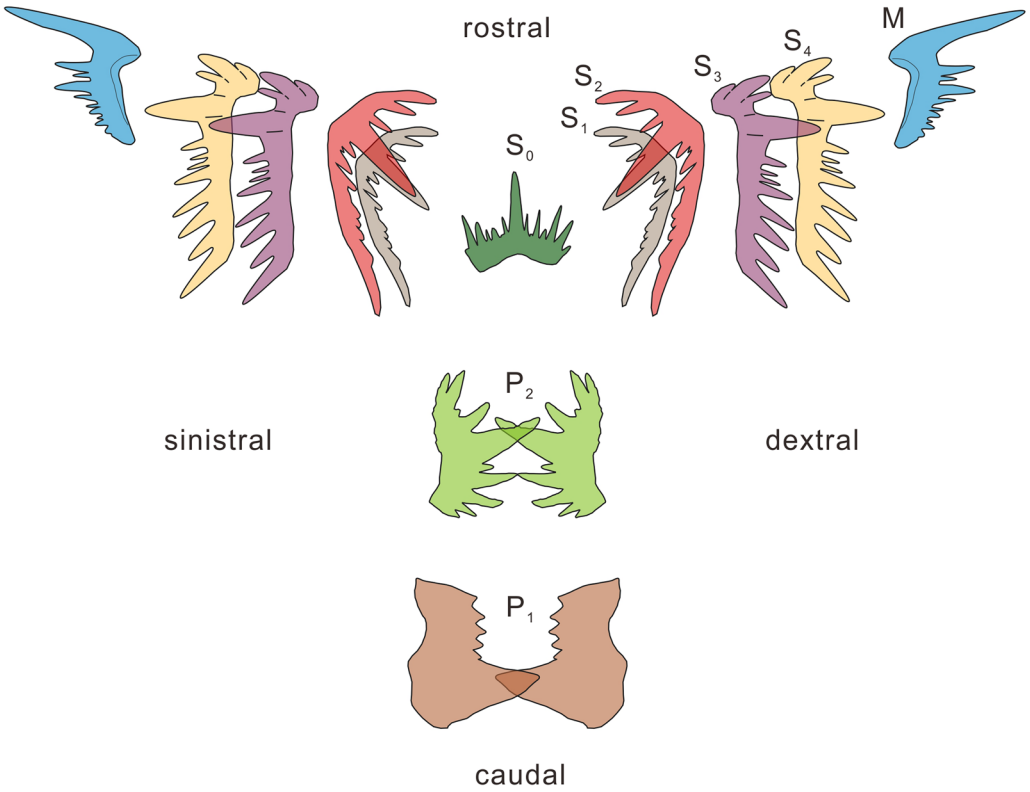

Fig. 6 The composition of the *H. parvus* apparatus based on conodont natural assemblages from the Shangsi section. Color coding follows Fig. 2

to tell the difference between S_1 and S_2 elements in our assemblages, however it seems that the 'short lateral' process is shorter in the S_1 than in the S_2 element (Fig. 5F).

Bipennate S_3 and S_4 elements. Both are laterally compressed with a long and robust cusp. The laterally flexed 'anterior' process is shorter than the 'posterior' process, bearing 2–4 denticles, the most distal of which is very large. The longer 'posterior' process is straight and bears 7–8 denticles, with the most distal one of which are enlarged.

The M element is dolabrate in shape. It has a long, robust, sharp cusp with a relatively long denticulate 'posterior' process and a weak anticusp at on the 'under side'. There is marked gap between the main cusp and the first of the denticles. The first denticle is longer than other delicate 'posterior' denticles. The 'posterior' process has a gentle incurvature. Of the M elements, many elements are described as the "makellate" forms in previous studies. However, according to the definition of the "makelliform" in Sweet (1988, P. 24–25), the "makelliform" elements include various pick-shaped forms (Sweet, 1988), such as, arched dolabrate, bipennate, breviform digyrate ramiform elements or geniculate coniform types. Therefore, we use the more specific term 'dolobrate' here.

The P_2 elements are angulate with a robust cusp, long or short 'anterior' and 'posterior' processes carrying several denticles of varying sizes. The sizes of the 'anterior' and 'posterior' processes vary among different the specimens. In specimen 2023SSCNA1, the 'posterior' process is approximately twice the length of the 'anterior' process (Fig. 3E), whereas in specimen 2023SSCNA2, the length of the 'anterior' and 'posterior' processes are similar (Fig. 4E). Not all denticles are the same size on the processes, in the sinistral P_2 element of specimen 2023SSCNA1, the second denticle is the largest of the 'anterior' process (Fig. 3E). Near the 'anterior' and 'posterior' ends of the 'posterior' process of the dextral P_2 element (Fig. 3E), the denticles are relatively large and long, while others are smaller. However, there is a pattern where some smaller second-order denticles intercalate between the bigger first-order denticles on the 'posterior' process of the dextral P_2 element. This pattern differs from the sinistral P_2 element in this assemblage with no second-order denticles (Fig. 3E). About the P_2 elements in specimen 2023SSCNA2 (Fig. 4E), the second and third denticles in the middle are the largest among the five denticles on the 'anterior' process. On the posterior process, the first and third denticles are larger than the other two.

The P_1 elements are carminiscaphate with a large upright cusp (Fig. 4C, 5E), followed by 6 small denticles arranged with triangular gaps between them. The 'posterior' edge is high, descending abruptly, nearly upright. The basal cavity is 'laterally' enlarged in the 'posterior' half, with a smooth 'upper surface'.

Discussion

Hindeodus was thought a seximembrate apparatus (Sweet, 1977, 1988), generally comprising the elements of carminiscaphate in P_1 (Pa) position, angulate in P_2 (Pb) position, makellate in M position, alate in S_0 (Sa) position, digyrate in $S_{1\text{-}2}$ (Sb) position, and bipennate in $S_{3\text{-}4}$ (Sc) elements position. However, the specific number of element constituting the multielement apparatus in this genus of *Hindeodus* was not clearly clarified. There are many restored apparatuses of *Hindeodus* in previous works (as shown in Table 1 of Agematsu et al., 2018) on the basis of the discrete elements. In these studies, it is noteworthy that Matsuda (1981) reconstructed a multielement apparatus of *H. minutus* and provided a detailed morphological explanation for each constituent element, with a particular emphasis on the orientation of those elements. Additionally, Kozur (1996) summarized the characteristics of some species in *Hindeodus* near the Permian–Triassic boundary, especially the species of *H. typical*, *H. latidentatus*, and *H. parvus*. He wrote that "*the ramiform elements in apparatus of* Hindeodus*, and partly the Sb (now $S_{1\text{-}2}$) elements are different enough to facilitate good species separation in those species in which the Pa (now P_1) element is not very diagnostic for separation from other species during the Carboniferous to Middle Permian, they are rather similar and partly overlap in their variability in different* Hindeodus *species*". However, most of them are based on discrete elements rather than natural assemblages, thus there remains a certain degree of inadequacy in proving the validity of these apparatuses, as each type requires validation through its corresponding natural assemblages.

Hindeodus parvus (*Anchignathodus parvus*) was firstly assigned to two ramiform elements in this apparatus (Kozur, 1975, 1977; Kozur & Piatakova, 1976), neoprioniodiniform element in M position and hindeodelliform element in Sc ($S_{3\text{-}4}$) position, respectively. This species has been widely discussed in recent studies, with a significant debate focusing on the number of the elements in its apparatus (Agematsu et al., 2018; Purnell et al., 2018). Three hypotheses regarding the apparatus composition of *Hindeodus* (*H. parvus*, *H. typicalis*) remain under consideration (Purnell et al., 2018): (A) that the apparatus is missing two S_1 elements with 7 S (S_0, $S_{2\text{-}4}$), 2 M, 2 P_2, and 2 P_1, in total 13 elements; (B) that the apparatus is missing two P_2 elements with 9 S (1 S_0, paired S_1-S_4), 2 M, and 2 P_1, in total 13 elements; or the hypothesis (C), that all those elements are present, showing a typical 15-element apparatus, including 1 S_0, paired S_1-S_4, 2 M, 2 P_2, and 2 P_1 elements. The primary reason for these discrepancies is likely the incomplete nature of the obtained fossil materials. In this context, in 2015, two apparatuses from the *Hindeodus* species, *H. typicalis* and *H. parvus*, were identified in Japan, proposing a typical ozarkodinid 15-element apparatus (Agematsu et al., 2015). However, only 13 elements were identified in those assemblages, missing the two S_1 elements. In these assemblages, interestingly, the shape of the P_2 elements closely resembled the morphology of the S elements (Zhang et al., 2017).

In 2017, a 13-element apparatus of *H. parvus* was proposed based on six fused clusters from the Bed 32 in the Shangsi section (Zhang et al., 2017), which included a complete 9-element S array, differing from the apparatus of *H. parvus* established in Japan. The main difference of this proposal compared with previous one was the loss of the two P_2 elements, interpreted by the authors as a possible functional change in the food processing ability of the apparatus after the end Permian mass extinction.

Soon later in 2017, a completely natural assemblage of *H. parvus* was presented (Agematsu et al., 2017). The new evidence showed that the apparatus of *H. parvus* comprised a 15 elements composition. The natural assemblage contained the S_1 pair as well as the two P_2 elements, situated between the caudal halves of the sinistral and dextral S elements in the natural assemblage, closely resembled those elements described in Agematsu et al. (2015).

The debate in the above studies primarily revolves around the existence of P_2 elements in the *Hindeodus* apparatus. Zhang et al. (2017) did not discover the P_2 elements in the materials of fused clusters or individual conodont elements, whereas the P_2 element morphology presented by Agematsu et al. (2015) closely resembles a ramiform element (interpreted as S_1 elements by Zhang et al., 2017). Furthermore, Agematsu et al. (2015) did not detect S_1 elements in the natural assemblages, leading to the conclusion that this type of multielement apparatus in *Hindeodus* constitutes a 13-element apparatus. Although Agematsu et al. (2017) showcased a more complete natural assemblage interpreted through CT scanning, featuring both S_1 and P_2 elements in a 15-element apparatus, the P_2 element in their study is also quite similar to a ramiform element, as observed in Agematsu et al. (2015). Unfortunately, the relevant CT data were not appended along with the article, hindering the verification of data completeness. It is generally agreed upon that the S-M element group (1 S_0, 2 S_1, 2 S_2, 2 S_3, 2 S_4, and 2 M) comprises 11 elements (Agematsu et al., 2015, 2017; Zhang et al., 2017). Currently, we have unequivocally

identified a pair of P_2 elements with consistent morphology in two specimens. This P_2 element pair stands out distinctly from the P_2 elements presented by Agematsu et al., (2015, 2017) and other reconstructions before (Supp. Table 1 here and Table 1 in ref. Agematsu et al., 2018) and belongs to the true angulate elements, characterized by a large cusp situated in the middle of the unit, slightly convex outside, and a curve upwards along their lower edge. There is no question that this morphological type does not classify as a ramiform element, signifying that our discovery has resolved this long-standing debate.

The new preserved natural assemblages of *H. parvus* here reported, although apparently did not show all the elements, they clearly display the dextral S_1, S_2, S_3 and S_4 elements, and pairs of P_2 and P_1 elements in specimen 2023SSCNA2 (Figs. 4, 5), and a single S_0 element and paired P_2 elements in specimen 2023SSCNA1 (Figs. 2, 3). Based on the characteristic symmetry of the apparatus, it clearly shows that the *H. parvus* apparatus indeed consists of 15 elements in total, being consistent with the typical ozarkodinid 15-element template, with 9 S, 2 M, 2 P_2 and 2 P_1 elements (Fig. 6). The S_0 element is one alate form, the S_1 and S_2 elements are two paired similar digyrate forms, the S_3 and S_4 elements are two paired similar bipennate forms, the M elements are paired dolobrate forms, and the P_2 and P_1 elements are paired angulate and carminiscaphate forms, respectively.

Overall, currently reconstructed *H. parvus* apparatus shows that the morphological types of the elements are generally consistent, but there are some small morphological differences among the elements (Supp. Table 1). The discovery of the new natural assemblages gives us an opportunity to discuss the different morphology of elements in the *Hindeodus* multielement apparatus.

The S_0 elements are almost similar in all reconstructions, with a thin symmetrical body unit, a large and long cusp at the middle, and two 'lateral' processes bearing irregular sized denticles, beside the cusp there are always four or more small denticles and the distal denticles on both side processes are larger than those denticles near the cusp, and the unit is slightly or strongly convex 'anteriorly'. There are some distinct differences of S_0 elements in different species of the *Hindeodus*: the lower surface is flat (Agematsu et al., 2018; Jiang, 2008; Kozur, 1995, 1996; Li et al., 1989; Yang et al., 2014), or slightly to strongly arched upwards (Agematsu et al., 2015, 2017; Clark et al., 1981; Matsuda, 1981; Sweet, 1977; Zhang & Yang, 1991; Zhang et al., 2017; this paper), forming the center angle of 180 to 90 degrees between lower surfaces of two 'lateral' processes (Sweet, 1977); the distal end of the lower surface is rounded in some specimens (Agematsu et al., 2015, 2017, 2018; Matsuda, 1981; Yang et al., 2014; Zhang et al., 2017) and subanguler in others (Clark et al., 1981; Sweet, 1977; this paper). The thickness of the unit, robustness of cusp and denticles, and curvature of the lower surface below the cusp will affect the identification for the different species. However, interesting, clearly different shapes were assigned to S_0 elements in the same species of *H. parvus* (Supp. Table 1).

On the other hand, the S_1 and S_2 elements are similar in shape, consisting of a digyrate element with long and short processes forming an angle of *ca.* 110° (Fig. 5F) (Zhang et al., 2017). The long process points caudo-dorsally in the apparatus, while the short process points the inner side of the apparatus. This characteristic could be also observed in other figured material (Supp. Table 1; text Figs. 8, 9D, E in ref. Zhang et al., 2017 and text Fig. 4 in ref. Agematsu et al., 2017). According to the description of the element terminology by Sweet (1977) and Matsuda (1981), the process carrying the cusp is referred as the 'posterior' process, while the other process is known as the 'anterior' process. In $S_{1\text{-}2}$ elements, the inward curvature of the 'anterior' process begins closer to the cusp (see Supp. Table 1). Kozur (1996) notes that the strongly inward-curved part includes not only the 'anterior' process or its anterior portion but also the moderately large cusp and, in some cases, even the first denticle of the 'posterior' process in the $S_{1\text{-}2}$ (Sb) elements of *H. parvus*. However, in current reconstructions, these special features have not been observed in natural assemblages of *H. parvus* and their accompanying discrete $S_{1\text{-}2}$ elements (Agematsu et al., 2015, 2017; Jiang, 2008; Zhang et al., 2017). It suggests that this characteristic is not unique to *H. parvus*, possibly due to the collection of discrete elements.

Regarding the S_1 and S_2 elements, Kozur (1996) points out that the outline of $S_{1\text{-}2}$ (Sb) element is very important to separate the different species in *Hindeodus* because the typical feature of its curved curvature other than those hardly diagnostic Pa (P_1) elements from other species. Upon examining the reconstructions, particularly those elements from the Carboniferous such as *H. cristulus* (Sweet, 1977; Von Bitter & Plint-Geberl, 1982), it is evident that their shapes differ significantly from those found in the Permian and Early Triassic periods. The elements of $S_{1\text{-}2}$ (Sb) from the Carboniferous, their 'posterior' processes are short, slightly downward, and curve near the end of the 'posterior' process, while the 'anterior' processes curve close to the cusp and abruptly upward. In contrast, the two processes of Triassic $S_{1\text{-}2}$ elements, their 'anterior' process curving near the cusp (Zhang & Yang, 1991).

The S_3 and S_4 elements are similar to each other, with a 'long posterior' process and a 'lateral' curvature 'anterior' process, forming an angle of *ca.* 100° (Fig. 5F). Our specimens have 7–8 small denticles ornamenting the

'posterior' process, meanwhile in other figured materials, can be clearly recognize up to 15 small denticles (text Figs. 2–4 in Agematsu et al., 2015; text Figs. 6, 9F, G in Zhang et al., 2017; and text Fig. 4 in Agematsu et al., 2017). In contrast, other specimens show fewer denticles (only four denticles) on the 'posterior' process with wide intervals (text Fig. 3 in Zhang et al., 2017), suggesting that they might belong to different species. Additionally, the number of denticles and the curvature of the 'anterior' process vary among different specimens, ranging from one to four denticles, and exhibiting both, weak and strong 'lateral-curved' short process (Agematsu et al., 2017; Li et al., 1989; Matsuda, 1981; Zhang et al., 2017). Other reconstructions of the S_{3-4} (Sc) elements typically exhibit a short 'anterior' process that curves slightly inward and downward, located just ahead of the cusp (see Supp. Table 1; Matsuda, 1981). This process is characterized by one to three small denticles preceding the cusp, in addition to a larger, terminal denticle that extends more forward than it does backward. The cusp is significantly long and slender. The 'posterior' process is elongated and sometimes bears more than twenty needle-like denticles of varying sizes, which incline 'posteriorly'; its last one or two denticles are larger than the rest.

The M element consists of a dolobrate element with a large cusp forming a short anticusp, and a gentle curved 'posterior' process. This anticusp feature could be observed in specimens from Agematsu et al. (2017), but not in Zhang et al. (2017). The M element exhibits a 90° angle formed by the proximal and distal parts of the process in oral view (see text Fig. 9A, B in Zhang et al., 2017). However, such angle between the cusp and the 'posterior' process is less pronounced in Agematsu et al. (2017)'s material and our specimens. Additionally, the second denticle is slender and very long on the 'posterior' process in our M elements, which is not observed in the specimens of other studies. This difference may be attributed to damage to the denticles on the 'posterior' processes. In previous reconstructions of M elements, some exhibit a prominent anticusp (Agematsu et al., 2015; Matsuda, 1981; Wardlaw et al., 2015; Sweet, 1977; Yang et al., 2014; Zhang & Yang, 1991; among others), characterized by a strongly inward curvature following the cusp (Matsuda, 1981; Yang et al., 2014; Zhang et al., 2017). Some M elements show their lower surface of the basal pit distinctly everted (Matsuda, 1981; Von Bitter & Plint-Geberl, 1982; Wardlaw et al., 2015).

In the 2023SSCNA2 assemblage, the P_2 element has nearly equal lengths of the 'anterior' and 'posterior' processes, with 5 and 4 denticles respectively. However, in the specimen of 2023SSCNA1, the 'posterior' process of the P_2 element is clearly longer than the 'anterior' process, with respectively 8 and 11 small denticles on the 'posterior' process of the sinistral and dextral P_2 elements, and only 3 denticles on the anterior process in both the sinistral and dextral elements. This differences in the length of the processes are also observed in other figured P_2 elements (e.g. text Fig. 3–5 in ref. Agematsu et al., 2015; and text Fig. 4 in ref. Agematsu et al., 2017). Other reconstructions of P_2 (Pb) elements typically feature a short 'anterior' process bearing one or two denticles. The 'posterior' process is longer than the 'anterior' one, characterized by denticles of varying sizes, exhibiting a minor degree of torsion. The cusp is notably large and broad. However, the morphology of the P_2 elements we discovered differs from all previously P_2 morphologies (Supp. Table 1 and the reconstructions shown in Table 1 of the ref. Agematsu et al., 2018). The realness of P_2 elements of these earlier reconstructions still requires validation with the aid of more specimens from their natural assemblages.

The P_1 element has a high, upright cusp followed by 6 small denticles with pointed, rounded tips of similar size and height, a high 'posterior' edge, abruptly descending, and the basal cavity expands 'laterally' at a 'posterior' half of the unit with a smooth upper side surface. In our specimen, the cusp of P_1 element is especially high, nearly twice height of the small denticles to the lower margin, and significantly higher than other specimens (Agematsu et al., 2015, 2017; Zhang et al., 2017).

In summary, at present, it is hard to determine the evolutionary patterns of multielement apparatuses within the genus *Hindeodus* by examining subtle variations in element composition at different positions, such as the length of the unit, the thickness of the body, the number of denticles on the processes, the curvature of the process, or the angle of the lower margin. Although with the support of natural assemblages, the morphological characteristics of each constituent element in the restored *H. parvus* apparatus still show significant variability (Supp. Table 1), let alone those reconstructed apparatuses from isolated conodont elements. The ramiform elements that co-occur with *Hindeodus* indeed exhibit considerable morphological diversity, with the species of the early and late periods showing increasingly distinct characteristics among their constituent elements. Therefore, to adequately compare the differences among various apparatuses, we need to obtain more specimens of well-preserved natural assemblages for assistance; otherwise, many of the apparatuses currently reconstructed may still be significantly biased. Of course, those works are also significant, serving as a valuable reference for subsequent discussions.

H. parvus exhibits a typical 15-element apparatus characteristic of ozarkodinid conodonts. Interestingly, the slight morphological differences among the ramiform

and P_2 elements in the assemblages suggest that the currently reported specimens may belong to two different species of *Hindeodus*. This uncertainty could result from an incomplete understanding of other species within this genus, differences in the growth stages of the apparatus, or variations in living environments, therefore further work is needed in order to recover a better and more complete material to unravel these aspects.

Conclusions

The study of two conodont natural assemblages from the Lower Triassic strata at the Shangsi section in Guangyuan, Sichuan, reveal articulated remains of conodont skeletal apparatus. At least one assemblages provide direct evidence for the morphology, number, and topology of elements in the *Hindeodus parvus* apparatus. Integration of evidence from associated discrete elements (Li et al., 1989), fused clusters (Zhang et al., 2017), and natural assemblages (Agematsu et al., 2015, 2017) indicates that *H. parvus* possesses a nine-element S array (comprising an unpaired S_0 and paired S_1, S_2, S_3, and S_4 elements), along with two M, two P_2, and two P_1 elements. Notably, the elements in our specimens are slightly thicker than those in previously reconstructed models. Despite these differences, the *H. parvus* element arrangement remains highly conservative, maintaining the number, morphology, and topology of the well-established 15-element ozarkodinid model, although a relative high interspecific and intraspecific morphological variation can be recognized, that could be due to differences in the growth stages of the apparatus, or variations in living environments. In any case, our data suggest a basic, and very stable, model in the apparatus composition and architecture over more than 250 million years.

Supplementary Information

The online version contains supplementary material available at https://doi.org/10.1186/s13358-024-00337-2.

Additional file 1: Supplementary Table 1. The reconstructions of *Hindeodus parvus* multielement apparatus from the Early Triassic.

Acknowledgements

This work was supported financially by the National Natural Science Foundation of China (42472011, 42272030); Chinese Geological Survey projects (DD20230219); State Key Laboratory of Palaeobiology and Stratigraphy (Nanjing Institute of Geology and Palaeontology, CAS) (No. 193110). CMP was supported by the Project of the Ministry of Science and Innovation of Spain (PID2020-117373GA-I00). We thank Wang Guan and Wang Kunyang for scanning the SEM images. We are grateful to Duncan Murdock and other two anonymous referees for their comments and positive suggestions.

Author contributions

JH, JL and CMP conducted field work, JH performed conodont research, analyzed data, and wrote the manuscript; SH, CMP, CZ, QZ, WW, XM, HJ, KZ revised the paper.

Data availability

No datasets were generated or analysed during the current study.

Declarations

Competing interests

We have no competing interests.

Received: 24 July 2024 Accepted: 1 October 2024
Published online: 02 December 2024

References

Agematsu, S., Golding, M. L., & Orchard, M. J. (2018). Comments on: Testing hypotheses of element loss and instability in the apparatus composition of complex conodonts (Zhang et al.). *Palaeontology, 61*, 785–792.

Agematsu, S., Sano, H., & Sashida, K. (2015). Natural assemblages of *Hindeodus* conodonts from a Permian-Triassic boundary sequence, Japan. *Palaeontology, 57*, 1277–1289.

Agematsu, S., Uesugi, K., Sano, H., & Sashida, K. (2017). Reconstruction of the multielement apparatus of the earliest Triassic conodont, *Hindeodus parvus*, using synchrotron radiation X-ray micro-tomography. *Journal of Paleontology, 91*, 1220–1227.

Aldridge, R. J., Briggs, D. E. G., Smith, M. P., Clarkson, E. N. K., & Clark, N. D. L. (1993). The anatomy of conodonts. *Philosophical Transactions of the Royal Society of London, Series b, Biological Sciences, 340*, 405–421.

Chen, Y., Jiang, H., Ogg, J. G., Wignall, P. B., & Lai, X. (2024). Latest Permian and earliest Triassic geomagnetic polarity timescale: A polarity reversal marks the greatest mass extinction. *Global and Planetary Change, 233*, 104368.

Clark, D.L., Sweet, W.C., Bergström, S.M., Klapper, G., Austin, R.L., Rhodes, F.H.T., Müller, K.J., Ziegler, W., Lindström, M., Miller, J.F. & Harris, A.G. (1981). *Treatise on invertebrate paleontology. Part w, miscellanea. Supplement 2 conodonta*. Geological Society of America and University of Kansas, Boulder, Colorado, and Lawrence, Kansas.

Demo, F. (2017). *Analysis of synchrotron microtomography 3D images of exceptional fused cluster of Mockina slovakensis (Conodonts)*. Master thesis, Università degli Studi di Padova, Italy.

Donoghue, P. C. J., & Purnell, M. A. (1999). Mammal-like occlusion in conodonts. *Paleobiology, 25*, 58–74.

Donoghue, P. C. J., Purnell, M. A., Aldridge, R. J., & Zhang, S. (2008). The interrelationships of 'complex' conodonts (vertebrata). *Journal of Systematic Palaeontology, 6*, 119–153.

Ferretti, A., Bancroft, A. M., & Repetski, J. E. (2020). GECkO: Global Events impacting COnodont evolution. *Palaeogeography, Palaeoclimatology, Palaeoecology, 549*, 109677.

Goudemand, N., Orchard, M. J., Tafforeau, P., Urdy, S., Brühwiler, T., Brayard, A., Galfetti, T., & Bucher, H. (2012). Early Triassic conodont clusters from South China: Revision of the architecture of the 15 element apparatuses of the superfamily Gondolelloidea. *Palaeontology, 55*, 1021–1034.

Goudemand, N., Orchard, M. J., Urdy, S., Bucher, H., & Tafforeau, P. (2011). Synchrotron-aided reconstruction of the conodont feeding apparatus and implications for the mouth of the first vertebrates. *Proceedings of the National Academy of Sciences of the United States of America, 108*, 8720–8724.

Henderson, C. M. (2018). Permian conodont biostratigraphy. The Permian Timescale. *Geological Society, London, Special Publications, 450*, 119–142.

Huang, J., Hu, S., Zhang, Q., Donoghue, P. C. J., Benton, M. J., Zhou, C., Martínez-Pérez, C., Wen, W., Xie, T., Chen, Z., Luo, M., Yao, H., & Zhang, K. (2019a). Gondolelloid multielement conodont apparatus (*Nicoraella*) from the Middle Triassic of Yunnan Province, southwestern China. *Palaeogeography, Palaeoclimatology, Palaeoecology, 522*, 98–110.

Huang, J., Martínez-Pérez, C., Hu, S., Donoghue, P. C. J., Zhang, Q., Zhou, C., Wen, W., Benton, M. J., Luo, M., Yao, H., & Zhang, K. (2019b). Middle Triassic conodont apparatus architecture revealed by synchrotron X–ray microtomography. *Palaeoworld, 28*, 429–440.

Huang, J., Martínez Pérez, C., Hu, S., Zhang, Q., Zhang, K., Zhou, C., Wen, W., Xie, T., Benton, M. J., Chen, Z. Q., Luo, M., & Donoghue, P. C. J. (2019c).

Apparatus architecture of the conodont *Nicoraella kockeli* (Gondolelloidea, Prioniodinina) constrains functional interpretations. *Palaeontology, 62*, 823–835.

Huang, J., Martínez-Pérez, C., Zhang, Q., Zhang, K., Luo, M., Wen, W., Zhou, C., Min, X., Ma, Z., Xie, T., Benton, M. J., & Donoghue, P. C. J. (2023). Exceptionally preserved conodont natural assemblages from the Middle Triassic Luoping biota, Yunnan Province, China: Implications for the architecture of conodont apparatus. *Journal of Earth Science, 34*, 1762–1776.

Hu, S., Feldmann, R. M., Schweitzer, C. E.,Benton, M. J., Huang, J., Wen, W., Min, X., Zhang, Q., Zhou, C., & Ma. Z., 2022. A new horseshoe crab from the Permian-Triassic transition of South China: Xiphosurids as key components of post-extinction trophic webs. Palaeogeography, Palaeoclimatology, Palaeoecology, 602:111178.

Jiang, H. (2008). *Research on conodont evolution across the Permian–Triassic Boundary in South China*. Ph.D. thesis, China University of Geosciences, Wuhan.

Jiang, H., Lai, X., Yan, C., Aldridge, R. J., Wignall, P., & Sun, Y. (2011). Revised conodont zonation and conodont evolution across the Permian-Triassic boundary at the Shangsi section, Guangyuan, Sichuan, south China. *Global and Planetary Change, 77*, 103–115.

Kozur, H. (1975). Beiträge zur conodontenfauna des Perm. *Geologisch Paläeontologische Mitteilungen Innsbruck, 5*, 1–44.

Kozur, H. (1977). Revision der Conodontengattung Anchignathodus und ihrer Typusart. *Zeitschrift Für Geologische Wissenschaften, 5*, 1113–1127.

Kozur, H. (1995). Some remarks to the conodonts *Hindeodus* and *Isarcicella* in the latest Permian and earliest Triassic. *Palaeoworld, 6*, 64–77.

Kozur, H. (1996). The conodonts *Hindeodus*, *Isarcicella* and *Sweetohindeodus* in the uppermost Permian and lowermost Triassic. *Geologia Croatia, 49*, 81–115.

Kozur, H., & Pjatakova, M. (1976). Die Conodontenart Anchignathodus parvus n. sp., eine wichtige Leitform der basalen Trias von Nord- und Zentraliran. *Koninklijke Nederlandse Akademie Van Wetenschappen-Amsterdam, Reprinted from Proceedings, Series B, 79*, 123–128.

Kozur, H. W. (1989). Significance of events in conodont evolution for the Permian and Triassic stratigraphy. *Courier Forschungsinstitut Senckenberg, 117*, 385–408.

Lai, X., Yang, F., Hallam, A., & Wignall, P. B. (1996). The Shangsi section, candidate of the Global Stratotype Section and point of the Permian-Triassic boundary. In H. Yin (Ed.), *The Palaeozoic-Mesozoic Boundary, Candidates of Global Stratotype Section and Point of the Permian-Triassic boundary* (pp. 113–124). China University of Geosciences Press.

Li, Z., Zhan, L., Dai, J., Jin, R., Zhu, X., Zhang, J., Huang, H., Xu, D., Yan, Z., & Li, H. (1989). *Study on the Permian-Triassic biostratigraphy and event stratigraphy of Northern Sichuan and Southern Shaanxi*. Geological Publishing House.

Martínez-Pérez, C., Rayfield, E. J., Botella, H., & Donoghue, P. C. J. (2016). Translating taxonomy into the evolution of conodont feeding ecology. *Geology, 44*, 247–250.

Martínez-Pérez, C., Rayfield, E. J., Purnell, M. A., & Donoghue, P. C. J. (2014). Finite element, occlusal, microwear and microstructural analyses indicate that conodont microstructure is adapted to dental function. *Palaeontology, 57*, 1059–1066.

Matsuda, T. (1981). Early Triassic conodonts from Kashmir, India. Part 1: *Hindeodus* and *Isarcicella*. *Journal of Geosciences, Osaka City University, 24*, 75–108.

Nicoll, R. S., Metcalfe, I., & Wang, C. Y. (2002). New species of the conodont genus *Hindeodus* and the conodont biostratigraphy of the Permian-Triassic boundary interval. *Journal of Asian Earth Sciences, 20*(6), 609–631.

Orchard, M. J. (2010). Triassic conodonts and their role in stage boundary definition. *Geological Society London, Special Publications, 334*, 139–161.

Purnell, M. A. (1995). Microwear on conodont elements and macrophagy in the first vertebrates. *Nature, 374*, 798–800.

Purnell, M. A., & Donoghue, P. C. J. (1998). Skeletal architecture, homologies and taphonomy of ozarkodinid conodonts. *Palaeontology, 41*, 57–102.

Purnell, M. A., & Jones, D. (2012). Quantitative analysis of conodont tooth wear and damage as a test of ecological and functional hypotheses. *Paleobiology, 38*, 605–626.

Purnell, M. A., & Von Bitter, P. H. (1992). Blade–shaped conodont elements functioned as cutting teeth. *Nature, 359*, 629–631.

Purnell, M. A., Donoghue, P. C. J., & Aldridge, R. J. (2000). Orientation and anatomical notation in conodonts. *Journal of Paleontology, 74*, 113–122.

Purnell, M. A., Zhang, M., Jiang, H., & Lai, X. (2018). Reconstruction, composition and homology of conodont skeletons: A response to agematsu et al. *Palaeontology, 61*, 793–796.

Song, H., Wignall, P. B., Tong, J., & Yin, H. (2013). Two pulses of extinction during the Permian-Triassic crisis. *Nature Geoscience, 6*(1), 52–56.

Sun, Y., Joachimski, M. M., Wignall, P. B., Yan, C., Chen, Y., Jiang, H., Wang, L., & Lai, X. (2012). Lethally hot temperatures during the early Triassic greenhouse. *Science, 338*, 366–370.

Sun, Z., Liu, S., Ji, C., Jiang, D., & Zhou, M. (2020). Synchrotron–aided reconstruction of the prioniodinin multielement conodont apparatus (*Hadrodontina*) from the lower Triassic of China. *Palaeogeography, Palaeoclimatology, Palaeoecology, 560*, 109913.

Sun, Z., Liu, S., Ji, C., Jiang, D., & Zhou, M. (2021). Gondolelloid multielement conodont apparatus (*Scythogondolella*) from the lower Triassic of Jiangsu, East China, revealed by high-resolution X-ray microtomography. *Palaeoworld, 30*, 286–295.

Sweet, W. C. (1977). Genus *Hindeodus* Rexroad & Furnish, 1964. In W. Ziegler (Ed.), *Catalogue of conodonts III* (pp. 203–224). E. Schweizerbart'sche Verlagsbuchhandlung.

Sweet, W. C. (1988). *The conodonta: Morphology, taxonomy, paleoecology, and evolutionary history of a long-extinct animal phylum*. Oxford University Press.

Sweet, W. C., & Donoghue, P. C. J. (2001). Conodonts: Past, present, future. *Journal of Paleontology, 75*, 1174–1184.

Takahashi, S., Yamakita, S., & Suzuki, N. (2019). Natural assemblages of the conodont *clarkina* in lowermost Triassic deep–sea black claystone from northeastern Japan, with probable soft–tissue impressions. *Palaeogeography, Palaeoclimatology, Palaeoecology, 524*, 212–229.

Von Bitter, P. H. V., & Plint-Geberl, H. A. (1982). Conodont biostratigraphy of the Codroy Group (Lower Carboniferous), southwestern Newfoundland, Canada. *Canadian Journal of Earth Sciences, 19*, 193–221.

Wardlaw, B. R., Nestell, M. K., Nestell, G. P., Ellwood, B. B., & Lan, L. T. P. (2015). Conodont biostratigraphy of the Permian-Triassic boundary sequence at Lung Cam, Vietnam. *Micropaleontology, 61*, 313–334.

Wignall, P. B., Hallam, A., Lai, X., & Yang, F. (1995). Palaeoenvironmental changes across the Permian/Triassic boundary at Shangsi (N. Sichuan, China). *Historical Biology, 10*, 175–189.

Yang, B., Yuan, D., Henderson, C. M., & Shen, S. (2014). *Parafurnishius*, an Induan (Lower Triassic) conodont new genus from northeastern Sichuan Province, southwest China and its evolutionary implications. *Palaeoworld, 23*, 263–275.

Yin, H., Yang, F., Zhang, K., Yang, W., & Cassinis, G. (1986). A proposal to the biostratigraphic criteria of Permian/Triassic boundary. *Memorie Della Societa Geologica Italiana, 34*, 329–344.

Yin, H., Zhang, K., Tong, J., Yang, Z., & Wu, S. (2001). The global stratotype section and point (GSSP) of the Permian-Triassic boundary. *Episodes, 24*, 102–114.

Zeng, W., Purnell, M. A., Jiang, H., & Zhang, M. (2021). Late Triassic (Norian) conodont apparatuses revealed by conodont clusters from Yunnan province, southwestern china. *Journal of Earth Science, 32*, 709–724.

Zhang, K., Tong, J., Shi, G. R., Lai, X., Yu, J., He, W., Peng, Y., & Jin, Y. (2007). Early triassic conodont–palynological biostratigraphy of the Meishan D section in Changxing, Zhejiang province, South China. *Palaeogeography, Palaeoclimatology, Palaeoecology, 252*, 4–23.

Zhang, M., Jiang, H., Purnell, M. A., & Lai, X. (2017). Testing hypotheses of element loss and instability in the apparatus composition of complex conodonts: Articulated skeletons of *Hindeodus*. *Palaeontology, 60*, 595–608.

Zhang, S., & Yang, Z. (1991). *On multielement taxonomy of the early. Triassic conodonts stratigraphy and paleontology of China* (pp. 17–47). Beijing: Geological Publishing House.

Zhao, L., Tong, J., Sun, Z., & Orchard, M. J. (2008). A detailed lower Triassic conodont biostratigraphy and its implications for the GSSP candidate of the Induan-Olenekian boundary in Chaohu, Anhui province. *Progress in Natural Science, 18*, 79–90.

Publisher's Note

Springer Nature remains neutral with regard to jurisdictional claims in published maps and institutional affiliations.